HEFAT2014
10^{th} International Conference on Heat Transfer, Fluid Mechanics and Thermodynamics
14 – 16 July 2014
Orlando, Florida

LOW-ORDER DISCRETE DYNAMICAL SYSTEM FOR H_2-AIR FINITE-RATE CHEMISTRY IN 3D

Zeng W.[a,*], Fu R.[a], and McDonough J. M.[b]
[a]Department of Mechanical Engineering
[b]Departments of Mechanical Engineering and Mathematics
University of Kentucky
Lexington, Kentucky, 40506
USA
E-mail: wenwei.zeng@uky.edu

ABSTRACT

A low-order discrete dynamical system (DDS) model for finite-rate chemistry of H_2-air combustion is derived in 3D. Simulation is performed in the context of a new subgrid-scale (SGS) method. Regime maps are used to determine useful ranges of values for bifurcation parameters. Specifically, a nine-step mechanism of H_2-air reactions with N_2-dilution is studied. As input to the DDS model, one fixed position within the flow chosen from Meier et al., is used (*Combustion Science and Technology*, 1996). The results in terms of time series of velocities, species mass fractions and the sum of mass fractions are analyzed. Moreover, the results are compared with experimental data at the selected position in the flame field. Discrepancies between computed and experimental results are discussed, and possible causes for discrepancies are analyzed. The potential of applying the current DDS in large-eddy simulation is addressed.

INTRODUCTION

Direct numerical simulation (DNS) is a method in computational fluid dynamics in which the Navier–Stokes equations are numerically solved without any turbulence model. DNS is a useful tool for fundamental research in turbulence, and it is possible to perform "numerical experiments" and extract from them information difficult or impossible to obtain in the laboratory, allowing a better understanding of the physics of turbulence. However, the computational cost of DNS is very high, even at low Reynolds numbers; and it is generally not possible for finite-rate chemistry except in two space dimensions. For Reynolds numbers encountered in most industrial applications, the computational resources required by a DNS would exceed the capacity of the most powerful computers currently available.

Presently, applying simple mathematical models to deal with turbulent combustion is a very common practice. The goal of modeling is to replace a complicated system of equations with a much simpler one that can be solved analytically, or with minimal numerical analytic effort. There are two widely-used classes of turbulent flow models, namely, Reynolds-averaged Navier–Stokes (RANS) and large-eddy simulation (LES). RANS methods have been successful in predicting some gross features of combustion, such as the profiles of combustor exit temperatures, whereas these are unable to predict transient phenomena such as flameout and relight in gas turbines, combustion instabilities in gas turbines and afterburners, cycle-to-cycle variations in IC engines, and pollutant formation, as noted by E. Fedina and C. Fureby [1]. Rather, the goal of RANS modeling in such situations is simply to produce averaged scalar fluxes whose overall effect is close to a "smearing" over time of the actual physics. This is unacceptable in many combustion studies.

It is well known that typical chemical reaction rates can be expressed in the form of the Arrhenius law [2]

$$k(T) = AT^n \exp\left(\frac{-E_a}{R_0 T}\right), \tag{1}$$

where E_a is activation energy, R_0 is the universal gas constant, T is temperature; and A and n are empirical constants. This form is extremely nonlinear, and must be averaged in the context of the RANS formalism or filtered in typical LES [3]. It is clear that

$$\overline{k}(T) = \overline{AT^n \exp\left(\frac{-E_a}{R_0 T}\right)}$$
$$\neq A\overline{T}^n \exp\left(\frac{-E_a}{R_0 \overline{T}}\right) = k(\overline{T}),$$

and the lack of equality is so severe that the second formula on the right simply cannot be used.

An alternative method to RANS for modeling combustion is LES. In LES, the large-scale energy-carrying motion is directly resolved on the grid, while the small-scale is modeled. The usual LES decomposition for the velocity $\boldsymbol{u}(\boldsymbol{x},t)$ is

$$\boldsymbol{u}(\boldsymbol{x},t) = \widetilde{\boldsymbol{u}}(\boldsymbol{x},t) + \boldsymbol{u}'(\boldsymbol{x},t)\,. \tag{2}$$

In this decomposition, $\widetilde{\boldsymbol{u}}(\boldsymbol{x},t)$ is usually termed the *large-* or *resolved-scale* part of the solution, and $\boldsymbol{u}'(\boldsymbol{x},t)$ is called the *small-scale*, *subgrid-scale*, or *unresolved* part. It is important to note that the resolved and unresolved scales depend on both space and time, and this is a major distinction and advantage in comparison with the Reynolds decomposition.

Most recent research in LES has focused on SGS models, which are especially problematic in the context of finite-rate chemistry at least in part due to use of so-called implicit filtering leading to the inequality shown earlier in the context of the reaction rate formula. But other forms of LES are beginning to be studied. A typical LES-like decomposition of solution variables employed in such formalisms is

$$\boldsymbol{Q}(\boldsymbol{x},t) = \boldsymbol{q}(\boldsymbol{x},t) + \boldsymbol{q}^*(\boldsymbol{x},t), \quad \boldsymbol{x}\in\mathbb{R}^d,\ \ d=2,3. \tag{3}$$

Substituting Eq. (3) into the transport equation(s) for the dependent variable vector $\boldsymbol{Q}$ results in

$$(\boldsymbol{q}+\boldsymbol{q}^*)_t + \nabla\cdot\boldsymbol{F}(\boldsymbol{q}+\boldsymbol{q}^*) = \nabla\cdot\boldsymbol{G}(\boldsymbol{q}+\boldsymbol{q}^*) + \boldsymbol{S}(\boldsymbol{q}+\boldsymbol{q}^*), \tag{4}$$

where $\boldsymbol{q}(\boldsymbol{x},t)$ is the large-scale part, and $\boldsymbol{q}^*(\boldsymbol{x},t)$ is the small-scale part; the subscript t denotes partial differentiation with respect to time, and $\nabla\cdot$ is the divergence operator. $\boldsymbol{F}$ and $\boldsymbol{G}$ are advective and diffusive fluxes, respectively, and $\boldsymbol{S}$ is a nonlinear source term.

A basic hypothesis regarding construction of the small-scale model is that $\boldsymbol{q}^*$ in Eq. (3) can be expressed as

$$q_i^* = A_i M_i, \qquad i=1,2,\ldots,N_v, \tag{5}$$

where, N_v is the total number of dependent variables; $\boldsymbol{q}_i^*$ is the i^{th} component of the N_v small-scale dependent variables; the A_is are amplitudes derived from scaling laws of Kolmogorov (see, e.g., Frisch [4]); and M_i is a chaotic map that can exhibit bifurcation leading to a strange attractor, thus producing small-scale turbulent temporal fluctuations locally in space and time [3].

In this paper, we will apply the method, originally proposed in 2D and studied by McDonough and Zhang [5] [6], to construct a 3-D SGS model for LES. This method includes the well-known logistic map

$$m^{(n+1)} = \beta m^{(n)}(1-m^{(n)})\,, \tag{6}$$

first presented by May [7], a widely-used model to deal with complicated dynamical systems. Frisch [4] demonstrated that a simple quadratic map,

$$x^{(n+1)} = 1 - 2x^{(n)}, \tag{7}$$

might be viewed as a *'poor man's Navier–Stokes equation'*, and this is a transformation of Eq. 6. Furthermore, McDonough and Huang [8] have derived the 2-D 'poor man's Navier–Stokes equation',

$$a^{(n+1)} = \beta_1 a^{(n)}(1-a^{(n)}) - \gamma_1 a^{(n)} b^{(n)}, \tag{8a}$$

$$b^{(n+1)} = \beta_2 b^{(n)}(1-b^{(n)}) - \gamma_2 a^{(n)} b^{(n)}, \tag{8b}$$

directly from the Navier–Stokes equations via a Galerkin procedure.

In this work, we will use an analogous approach in 3D to derive a finite-rate chemistry SGS model including the momentum and thermal energy equations similar to earlier studies in 2D in [8] and in [5] [6]. The purpose of this paper is to present a preliminary exploration of the behavior of this DDS for a specific reduced-kinetic mechanism for H_2-air combustion and to compare the computed results with extant experimental data.

In the remainder of this work, we present the governing equations and assumptions, derive the corresponding DDS for a specific reduced mechanism via a single-mode Galerkin approximation, and present results and compare these to experimental data.

MODEL

In this section, we will first introduce the governing equations, and from these derive a general DDS that can be used to model any desired chemical kinetics as well as other physics. Then, we provide a reduced mechanism for H_2-air combustion and introduce the experimental data to be used for comparison.

Governing Equations

The general governing equations used to describe combustion include equations for mass conservation, momentum balance, and energy and species transport. They are

$$\rho_t + \nabla\cdot(\rho\boldsymbol{U}) = 0, \tag{9a}$$

$$\rho\frac{D\boldsymbol{U}}{Dt} = -\nabla p + \nabla\cdot(\mu\nabla\boldsymbol{U}) + \rho\boldsymbol{g}, \tag{9b}$$

$$\rho c_p\frac{DT}{Dt} = \nabla\cdot(\lambda\nabla T) + \sum_{i=1}^{N_s} c_{p_i} D_i W_i \nabla\left(\frac{\rho Y_i}{W_i}\right)\cdot\nabla T - \sum_{i=1}^{N_s} h_i\dot{\omega}_i, \tag{9c}$$

$$\frac{D(\rho Y_i)}{Dt} = \nabla\cdot(\rho D_i\nabla Y_i) + \dot{\omega}_i, \qquad i=1,\ldots N_s. \tag{9d}$$

Here,

$$\dot{\omega}_i = W_i\sum_{j=1}^{N_r}(\nu''_{i,j} - \nu'_{i,j})\omega_j\,, \tag{10}$$

with

$$\omega_j = k_{f,j} \prod_{l=1}^{N_s} \left(\frac{\rho Y_l}{W_l} \right)^{\upsilon'_{i,j}} - k_{b,j} \prod_{l=1}^{N_s} \left(\frac{\rho Y_l}{W_l} \right)^{\upsilon''_{i,j}}. \quad (11)$$

These equations hold on a 3-D spatial domain $\Omega \in \mathbb{R}^3$ during a specified time interval $t \in (t_0, t_f)$, and $\boldsymbol{U} = (u, v, w)^T$; D/Dt is the substantial derivative; ∇ is the gradient operator; $\boldsymbol{g}$ is the body-force acceleration vector, ρ is density, and p is the pressure. T is temperature; Y_i is the mass fraction, and h_i is specific enthalpy, of species i. The transport properties include (dynamic) viscosity μ, thermal conductivity λ, and the binary diffusion coefficient D_i of species i in the ambient background gas. Here, c_{p_i} and W_i are the specific heat capacity and relative molecular mass of species i, respectively; $\nu'_{i,j}$ and $\nu''_{i,j}$ are stoichiometric coefficients of reactants and products corresponding to species i in reaction j. N_s and N_r are the number of species and reactions, respectively. Finally, $k_{f,j}$ and $k_{b,j}$ are the forward and backward reaction rate coefficients of the j^{th} reaction, respectively. The reaction rate expression was shown in Eq. (1), and we write the specific form for the j^{th} reaction:

$$k_j = A_j T^{n_j} \exp\left(\frac{-E_j}{R_0 T} \right).$$

Recall that in LES the large-scale part has been resolved directly, so we now propose to construct corresponding DDS SGS models from the governing equations. We then add the SGS solutions of the latter to the resolved solution to construct an approximation to the complete solution. Because the DDSs are computed in the absence of resolved-scale information here, we will not analyze initial and boundary conditions for the chosen spatial domain in the present work.

Construction of Dynamical Systems

In modeling the chaotic maps M_i of Eq. (5), we assume all solution variables possess (generalized) Fourier series representations [9]

$$q_i(\boldsymbol{x}, t) = \sum_{\boldsymbol{k}=1}^{\infty} a_{\boldsymbol{k},i}(t) \varphi_{\boldsymbol{k}}(\boldsymbol{x}), \qquad x \in \Omega, \quad \in [t_0, t_f], \quad (12)$$

where functions $\{\varphi_{\boldsymbol{k}}\}_{\boldsymbol{k}=1}^{\infty}$ are basis functions of the Galerkin approximation for the Fourier coefficients, $a_{\boldsymbol{k},i}$, of the i^{th} dependent variable. There are several requirements associated with these basis functions: 1) $\{\varphi_{\boldsymbol{k}}\}_{\boldsymbol{k}=1}^{\infty}$ is complete in $L^2(\Omega)$; 2) it is orthonormal; 3) it exhibits behavior similar to complex exponentials, $e^{i\boldsymbol{k}\cdot\boldsymbol{x}}$, with respect to differentiation.

Now, we consider this representation restricted to the subgrid scale. In general, the number of wavevectors required for adequate representation decreases quickly as the extent of the spatial domain is reduced. Thus, we can use only a few wavevectors to represent $\boldsymbol{q}^*$ in Eq. (3). In this paper, we choose a single wavevector $\boldsymbol{k}$ for simplicity.

Detailed derivation of the 2-D poor man's Navier–Stoker's equation has been provided in [8], with the corresponding 3-D case by Polly [10]. In this paper, for brevity, we only present an outline of this derivation. We substitute Eq. (12), the Fourier representations of the dependent variables, into the governing Eqs. (9). Then form inner products of each equation with every basis function and use orthonormality of $\{\varphi_{\boldsymbol{k}}\}$ (the same simplifications used in [8]) to construct the Galerkin ordinary differential equations (ODEs). This procedure yields an infinite ODE system to replace the original PDEs. Here, we will use a simple forward-Euler, single-step, explicit time integration procedure to perform the temporal discretization. After appropriate rescaling to account for a single wavenumber, we obtain the following 3-D DDS model of Eqs. (9):

$$a^{(n+1)} = \beta_u a^{(n)}(1 - a^{(n)}) - \gamma_{12} a^{(n)} b^{(n)} - \gamma_{13} a^{(n)} c^{(n)}, \quad (13a)$$

$$b^{(n+1)} = \beta_v b^{(n)}(1 - b^{(n)}) - \gamma_{21} a^{(n)} b^{(n)} - \gamma_{23} b^{(n)} c^{(n)}, \quad (13b)$$

$$c^{(n+1)} = \beta_w c^{(n)}(1 - c^{(n)}) - \gamma_{31} a^{(n)} c^{(n)} - \gamma_{32} b^{(n)} c^{(n)} + \alpha_T e^{(n)}, \quad (13c)$$

$$d_i^{(n+1)} = -(\beta_{Y_i} + \gamma_{uY_i} a^{(n+1)} + \gamma_{vY_i} b^{(n+1)} + \gamma_{wY_i} c^{(n+1)}) d_i^{(n)} + \dot{\omega}_i + d_{i,0} \qquad i = 1, 2, \ldots, N_s, \quad (13d)$$

$$e^{(n+1)} = \left[\left(\sum_{i=1}^{N_s} \alpha_{Td_i} d_i^{(n+1)} - \gamma_{uT} a^{(n+1)} - \gamma_{vT} b^{(n+1)} - \gamma_{wT} c^{(n+1)} \right) e^{(n)} - \sum_{i=1}^{N_s} H_i \, \dot{\omega}_i \right] / (1 + \beta_T) + e_0, \quad (13e)$$

with

$$\dot{\omega}_i = \sum_{j=1}^{N_r} \left[C_{f,ij} \prod_{l=1}^{N_s} d_l^{\nu'_{j,l}} - C_{b,ij} \prod_{l=1}^{N_s} d_l^{\nu''_{j,l}} \right]. \quad (14)$$

Here, superscripts (n) are time-step indices; a, b, c, d_is, and e denote Fourier coefficients of the velocity vector in three directions, species concentrations, and temperature, respectively; the subscripted αs, βs, γs are DDS bifurcation parameters, all of which are associated with the various physical bifurcation parameters. For example, β_u, β_v, and β_w are functions of Reynolds number; α_T is related to Grashof number (actually, this term exists in all three velocity components); the α_{Td_i} are related to Schmidt and Lewis numbers; and the H_i are associated with specific enthalpies for each species i; the $C_{f,ij}$, $C_{b,ij}$ can be related to Kolmogorov-scale Damköhler numbers. The various γs correspond to velocity, temperature and species concentration gradients. The $d_{i,0}$s and e_0 are high-pass filtered species concentrations and temperature, respectively, for subgrid-scale behavior. We mention that for simplicity we will set α_T identically equal to zero in the present work, as buoyancy effects are negligible.

Reaction-Chemistry Reduced Mechanism

Overall (global) reactions are a consequence of collections of elementary reactions, and resolution of these elementary reactions is a difficult and time-consuming task [2]. Many elementary reactions produce a negligible contribution to the reaction process, and therefore can be ignored, leading to reduced mechanisms. Here, we only study the case of H_2-air reactions with N_2 dilution. Elementary reactions listed in Eqs. (15) are selected from the detailed H_2-O_2 reaction mechanism [11] and a reduced mechanism for H_2-air combustion [12]. The corresponding reaction rate data (assuming Arrhenius form) are listed in Table 1, where F means forward reaction and B means backward reaction.

Table 1. Reduced Mechanism for H_2-Air Reaction

#	F	A^a	n	E^a	B	A^a	n	E^a
a	k_f	3.52×10^{16}	-0.7	71.42	k_b	7.04×10^{13}	-0.26	0.60
b	k_f	5.06×10^{4}	2.67	26.32	k_b	3.03×10^{4}	2.63	20.23
c	k_f	1.17×10^{9}	1.3	15.21	k_b	1.28×10^{10}	1.19	78.25
d	k_0	5.75×10^{19}	-1.4	0.0	k_∞	4.65×10^{12}	0.44	0.0
e		7.08×10^{13}	0.0	1.23				
f	k_f	1.66×10^{13}	0.0	3.44	k_b	2.69×10^{12}	0.36	231.86
g		2.89×10^{13}	0.0	-2.08				
h	k_f	4.00×10^{22}	-2.0	0.0	k_b	1.03×10^{23}	-1.75	496.14
i	k_f	1.30×10^{18}	-1.0	0.0	k_b	3.04×10^{17}	-0.65	433.09

$$H + O_2 \rightleftharpoons OH + O \quad (15a)$$
$$H_2 + O \rightleftharpoons OH + H \quad (15b)$$
$$H_2 + OH \rightleftharpoons H_2O + H \quad (15c)$$
$$H + O_2 + M \rightharpoonup HO_2 + M^a \quad (15d)$$
$$HO_2 + H \rightharpoonup 2OH \quad (15e)$$
$$HO_2 + H \rightleftharpoons H_2 + O_2 \quad (15f)$$
$$HO_2 + OH \rightharpoonup H_2O + O_2 \quad (15g)$$
$$H + OH + M \rightleftharpoons H_2O + M^a \quad (15h)$$
$$2H + M \rightleftharpoons H_2 + M^a \quad (15i)$$

This mechanism is believed to be sufficient to describe premixed and nonpremixed flames, autoignition and detonations under conditions of practical interest. It consists of 15 reversible elementary reactions, and we collapse them to a nine-step mechanism, involving eight reacting species H_2, O_2, H_2O, OH, H, O, HO_2, N_2. Here, the bodies M and M^a are regarded as including all reacting species except the reactants/products of the particular reaction. For example, in reaction 15(d), M includes all of species except H and O_2, and the M^a includes all species except HO_2. Coefficients of reacting species are set to unity, which is different from the so-called San Diego mechanism [13].

Experimental Data

The experimental data are chosen from DLR Institute of Combustion Technology Experimental Data Archives, H_2/N_2 Jet Diffusion Flame [H3] (DLR Stuttgart), which is available at http://www.sandia.gov/TNF/simplejet.html. This flame was selected as a "standard flame" of the "International Workshop on Measurements and Computation of Turbulent Nonpremixed Flames," Naples, July 1996. It was investigated at the TU Darmstadt, Fachgebiet Energie-und Kraftwerkstechnik, and those data sets are available in the TU Darmstadt–Flame Data Base [14]. This is a nonpremixed flame with fuel ($50\%H_2 + 50\%N_2$, Reynolds number $=10000$, nozzle diameter $=8$mm, $V_{exit}=34.8$ m/s) and co-flowing air ($V_{air} = 0.3$ m/s). Meier *et al.* [15] provide a detailed description of this flame. We study the temperature and species concentrations at one specific point. Let x be the distance from the nozzle along the flame axis, D the nozzle diameter, and r the radial distance from the flame axis. The location considered in this work is $x/D = 2.5$ and $r = 6.75$mm; we note that this point is located where the temperature is maximum for the chosen x/D. The initial conditions, listed below, include temperature and mass fractions of four species in H_2-air combustion, namely, H_2, O_2, H_2O and N_2.

Table 2. Initial conditions: temperature and mass fractions

T [K]	Y_{H_2}	Y_{O_2}	Y_{H_2O}	Y_{N_2}
2095.6	0.0011	0.0531	0.1623	0.7834

RESULTS AND DISCUSSION

In this section, we consider a single position of the co-flow TU Darmstadt-Flame Data Base [14]. We calculate time series of velocities, temperature and species concentrations at this location using a low-order model based on the DDS described in an earlier section. We compare these computed results with the corresponding experimental data, provide a discussion regarding behavior of the computed results, and analyze the potential factors that may cause discrepancies between computation and experiment.

Regime Maps

For simplicity, the bifurcation parameters in Eqs. (13) are taken to correspond to homogeneous and isotropic turbulence. Namely, $\beta_u = \beta_v = \beta_w = \beta$, $\gamma_{12} = \gamma_{13} = \gamma_{21} = \gamma_{23} = \gamma_{31} = \gamma_{32} = \gamma$, and $\gamma_{uT} = \gamma_{vT} = \gamma_{wT} = \gamma_T$. We remark that neither the fluid flow nor the chemistry can be expected to be either homogenous or isotropic in this case, but this assumption provides a

tractable starting point. Moreover, we emphasize that no such assumption is needed in a complete LES because all bifurcation parameters can be calculated from high-pass filtered resolved-scale results. The values of these parameters associated with species i, e.g., β_{Y_i}, α_{Td_i} etc., should be analyzed individually since every species has its own characteristics. We present only one regime map, β vs. γ in Fig. 1. Once the different regimes are identified by their power spectral density (detailed analysis provided in Ref. [8]), we can choose regimes where chaotic-behavior is present, and apply the corresponding bifurcation parameters of the chaotic region in Eqs. (13) to evolve the DDS.

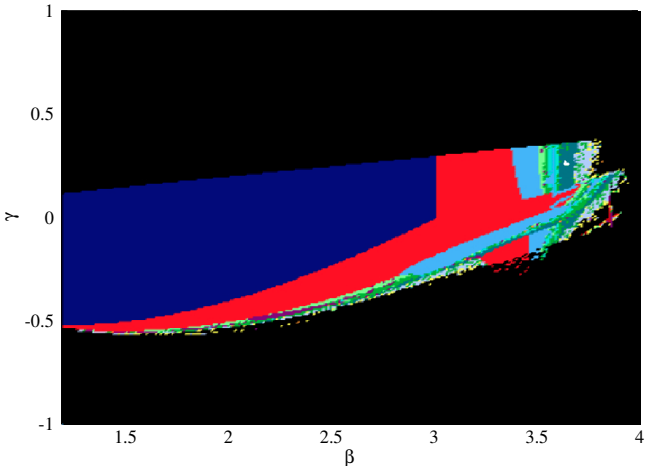

(a) Entire domain of interest

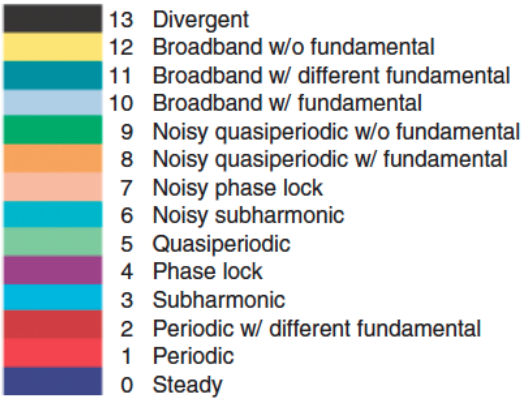

(b) color table

Figure 1. Regime map

In Fig. 1, we show the behaviors of the DDS for the parameters $(\beta, \gamma) \in [1.2, 4.0] \times [-1.0, 1.0]$. Specifically, the values $\beta = 3.6416$, $\gamma = 0.264$ are chosen, corresponding to the white point in the 11^{th} region of Fig. 1: broadband, essentially stochastic behavior, but with a fundamental frequency.

Validation of Model

In [5] 2-D DDS results for a similar combustion process are provided, but the more realistic 3-D case has not previously been studied. We will use the instantaneous sum of mass fraction fluctuations as a first measure to validate the model. Instead of forcing the sum to be unity by calculating all but one species and then setting it to satisfy the required unity value as is typical (and computationally more efficient), we directly calculate all species concentrations using the DDS and then observe the sum of mass fractions.

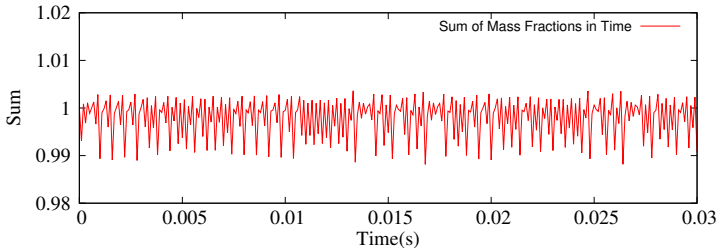

Figure 2. Sum of mass fractions vs. time

Figure 2 shows that the sum of mass fractions is close to unity for all times and the time averaged sum of mass fractions is 0.998, showing less than 1% discrepancy from the required value. Moreover, instantaneous values are nearly all greater than 0.99 and less than 1.002. These result show that the model works well in terms of mass fractions. In the following subsection, we will present additional computed results and compare them with experimental data to further validate this model.

Computed Results

Appropriate bifurcation parameters have been found as indicated in the subsection Regime Maps, and we use these in the DDS of Eq. (13) to obtain the computed results. The detailed comparison of computed results and experimental data is shown in Fig. 3 and Table 3, and we provide a brief discussion of the comparison.

Figure 3(a) shows that all five variables of the DDS exhibit turbulent behaviors, as is true for the experiments of Fig. 3(b), thus demonstrating that the DDS model can mimic the physical temporal turbulent fluctuations in a qualitative sense; but the fluctuation frequencies shown in Fig. 3(a) are higher than those of Fig. 3(b). A possible reason for the difference is that the fluctuation scale in the DDS model may be more sensitive than was the experimental equipment, and the former can generate smaller time scales. On the other hand, fluctuation amplitudes in Fig. 3(b) are higher than those of Fig. 3(a), which suggests a possible scaling problem in the model.

In Table 3, although the discrepancy of temperature is larger

than the experimental root mean square (RMS), the corresponding error is less than 10%. Furthermore, discrepancies of the four species in Table 3 are far less than the corresponding experimental RMS; and the largest error is less than 15%, which we view as acceptable for a low-order model to be used on the subgrid scale. Table 3 and Fig. 3 show that we nearly match mean values for species concentration, and the discrepancies are lower than the experimental RMS.

Table 3. Temperature and major species mass fraction mean values

	T [K]	Y_{H_2}	Y_{O_2}	Y_{H_2O}	Y_{N_2}
Experiment	2030.3	0.0012	0.0576	0.1565	0.7846
DDS model	2223.4	0.0010	0.0532	0.1601	0.7856
Experiment rms	85.4	0.0012	0.0188	0.0136	0.0081
Discrepancy	193.1	0.0002	0.0044	0.0036	0.0010
Error %	9.51	−14.53	−7.68	2.32	0.13

The temperature values in Table 3 and Fig. 3 are somewhat higher in the computation than in the experiment. This is due to the temperature model required for these calculations (small-scale plus large scale), which would not be needed in a complete LES. Overall, the computed results mimic the combustion process to a reasonable extent, and the 3-D DDS model works fairly well.

Discrepancy Analysis

Recall that the DDS model presented in this paper is derived for use as part of a SGS model for LES, and in this context would be evaluated at single points. So the computed results of the DDS model are set by initial conditions, and they do not account for behavior in the whole flow field. In contrast, although the experimental data are recorded at fixed positions, the species concentrations and temperature are affected by the fuel flow and air flow throughout the experiment.

The particular finite-rate reduced mechanism employed here is also a possible error source. Recall that we use only a nine-step mechanism (including forward and backward) for the combustion process, and this mechanism does not contain reactions for NO_x. We know NO_x exists at high temperature, and in this case the average temperature is over 2000K. Hence, we should possibly take NO_x reactions into consideration, and we will examine this in our continuing studies.

It is rather likely that the homogeneous, isotropic assumption is responsible for some, possible much, of the observed discrepancies. In [5] and [6], this assumption was not employed, and results were qualitatively better, even though the model was only 2D. Effects of this will also be investigated in ongoing studies.

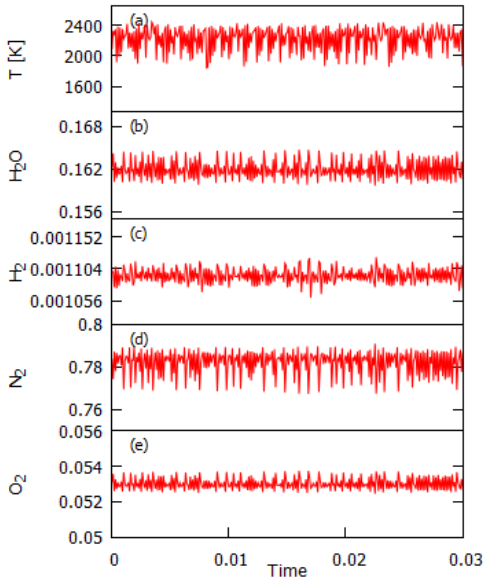

(a) DDS model

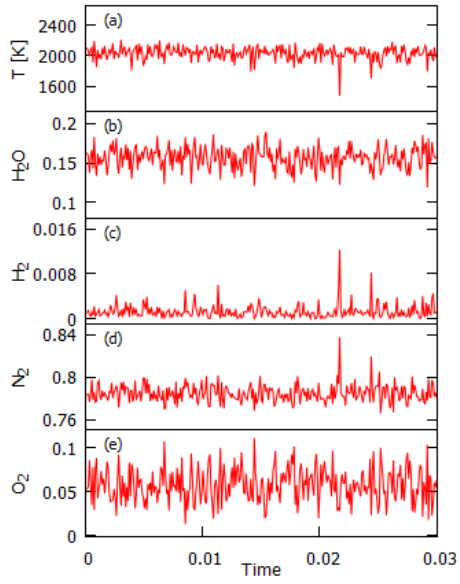

(b) Experimental Data

Figure 3. Comparison at x/D=2.5, r=6.75mm

CONCLUSIONS

In this paper we derived a 3-D discrete dynamical system for finite-rate combustion from governing PDEs and utilized this model with a nine-step reduced mechanism to mimic H_2-air combustion. The sum of species mass fractions close to unity demonstrates this model also works in 3D, as it previously did in 2D. Turbulent fluctuations exhibited in computed results are similar to those of experimental data in a qualitative sense; computed averaged temperature and species concentration are essen-

tially within experimental error. But the turbulence statistics and fluctuation amplitudes are not very accurate. However, we have mentioned that chosen bifurcation parameters did not necessarily agree with experimental data location conditions (in part due to the isotropy and homogeneity assumptions), and what we have attempted to do in this paper is model the combustion process rather than precisely duplicate a real physical situation. Furthermore, we are considering only a single location of flow field, and the DDS model provides a SGS simulation for this point only. For the whole flow field, we need to add this SGS model to the resolved part of a LES and thus construct an approximation to the complete solution. In the Discrepancy Analysis section, we find that the DDS model lost some information probably caused by several simplifications. We will study these shortcomings in further research.

In general, we believe the results of this study are sufficiently promising to suggest continued investigation of discrete dynamical systems for finite-rate chemistry as low-order models on subgrid-scales for large-eddy simulation.

REFERENCES

[1] Fedina E. and Fureby C., A comparative study of flamelet and finite rate chemistry LES for an axisymmetric dump combustor, *Journal of Turbulence*, **12**, 2011, pp. 1–20

[2] Warnatz Jürgen, Maas Ulrich., and Dibble R. W., *Combustion: Physical and Chemical Fundamentals, Modeling and Simulation, Experiments, Pollutant Formation*, 3^{rd} Edition, 2001.

[3] McDonough J. M., *Introductory Lectures on Turbulence Physics, Mathematics and Modeling*, Lecture notes, website of Advanced CFD Group. Retrieved from: http://www.engr.uky.edu/~acfd/lecturenotes1.html

[4] Frisch, U., TURBULENCE The Legacy of A. N. Kolmogorov, *Cambridge University Press*, Cambridge, 1995, pp. 89-92

[5] McDonough J. M. and Zhang Sha, Discrete dynamical systems models of turbulence-chemical kinetics interactions, 37^{th} *Intersociety Energy Conversion Engineering Conference*, Washington, DC, July 28–31, 2002.

[6] McDonough J. M. and Zhang Sha, LES subgrid-scale models of turbulence-chemical kinetics interactions based on discrete dynamical systems, 32^{th} *AIAA Fluid Dynamics Conference*, St. Louis, June 24–27, 2002.

[7] May R. M., Simple mathematical models with very complicated dynamics, *Nature*, **261**, 1976, pp. 459–467

[8] McDonough J. M. and Huang M. T., A 'poor man's Navier–Stokes equation': derivation and numerical experiments—the 2-D case, *Int. J. Numer. Meth. Fluids*, **44**, 2004, pp. 545–578

[9] McDonough J. M., *Lectures in Basic Computational Numerical Analysis*, Lecture notes. Retrieved from: http://www.engr.uky.edu/~acfd/lecturenotes1.html

[10] Polly James Bruce, *Numerical Experiments of the 3-D "Poor Man's Navier–Stokes Equations"*, MS Thesis, University of Kentucky, 2012.

[11] Li Juan, Zhao Zhenwei, Kazakov Andrei, and Dryer Frederick L., An updated comprehensive kinetic model of hydrogen combustion, *Int. J. Chemical Kinetics*, **36**, 2004, pp. 566–575

[12] Boivin P., Jiménez C., Sánchez A. L., Williams F. A., An explicit reduced mechanism for H_2-air combustion, 33^{rd} *International Symposium on Combustion*, January 8, 2010.

[13] Saxena P., Williams F. A., Testing a small detailed chemical-kinetic mechanism for the combustion of hydrogen can carbon monoxide, *Combustion and Flame*, **145**, 2006, pp. 316–323

[14] Schneider Ch., Dreizler A., Janicka J., and Hassel E. P., Flow Field Measurements of Stable and Locally Extinguishing Hydrocarbon-Fuelled Jet Flames, *Combustion and Flame*, **135**, 2003, pp. 185–190

[15] Meier W., Prucker S., Cao M. H., and Stricker W., Characterization of turbulent H_2/N_2/Air jet diffusion flames by single-pulse spontaneous Raman scattering, *Combustion Sci and Tech*, **118**, 1996, pp. 293–312